

## *Ab initio* dynamics of rapid fracture\*

Farid F Abraham†, D Brodbeck†, W E Rudge†, J Q Broughton‡,  
D Schneider§, B Land§, D Lifka§, J Germer§, M Rosenkrantz§, J Skovira§  
and H Gao||

† IBM Research Division, Almaden Research Center, San Jose, CA 95120, USA

‡ Naval Research Laboratory, Washington, DC 20375, USA

§ Cornell Theory Center, Cornell University, Ithaca NY, 14853, USA

|| Division of Mechanics and Computation, Stanford University, Stanford, CA 94305, USA

Received 20 October 1997, accepted for publication 8 January 1998

**Abstract.** As our title implies, we consider materials failure at the fundamental level of atomic bond breaking and motion. Using computational molecular dynamics, scalable parallel computers and visualization, we are studying the failure of notched solids under tension using in excess of  $10^8$  atoms. In rapid brittle fracture, two of the most intriguing features are the roughening of a crack's surface with increasing speed and the terminal crack speed which is much less than the theoretical prediction. Our two-dimensional simulations show conclusively that a dynamic instability of the crack motion occurs as it approaches one-third of the surface sound speed. This discovery provides an explanation for the crack's surface roughening and limiting speed. For three-dimensional slabs, we find that an intrinsically ductile FCC crystal can experience brittle failure for certain crack orientations. A dynamic instability also occurs, but brittle failure is not maintained. The instability is immediately followed by a brittle-to-ductile transition and plasticity. Hyperelasticity, or the elasticity near failure, governs many of the failure processes observed in our simulations and its many roles are elucidated.

'Refrain from immediately resorting to a jackhammer to break open a hazelnut without first checking for an incipient crack on the surface of the shell.' P-G de Gennes¶

'You may think I have used a hammer to crack eggs, but I have cracked eggs.' S Chandrasekhar+

### 1. Introduction

Historically, the classical physics of the continuum has provided most of the theoretical and computational tools for the engineer and the technologist, examples being elasticity, fluid dynamics and thermodynamics [1]. However, there is a new realization that understanding nanoscale behaviour is required where the continuum picture is no longer valid and that we must go to the domain of condensed-matter physics, statistical mechanics and quantum chemistry and in the broadest sense, to the nonlinear science of complex behaviour. This dichotomy of theoretical approaches may best be illustrated in the field of fracture dynamics by examining two recent advanced texts by Herrmann and Roux [2] and Freund [3]. With the advent of high-performance computers, the computational sciences of these disciplines are demonstrating the potential for providing very powerful tools and solutions of interest to materials failure. We will illustrate this by studying the dynamics of rapid fracture at

\* Based on Plenary Talk given at PC'97 by FFA.

¶ de Gennes P-G 1996 *Fragile Objects* (New York: Springer) p 58

+ From Rees M 1997 *Before the Beginning* (Reading, MA: Addison-Wesley) p 97

the atomistic level. While we will emphasize our studies, the non-equilibrium mechanics of liquids and solids is an active area of investigation by many computational scientists, Hoover being a prominent pioneer for the last three decades [4].

Continuum fracture theory typically assumes that cracks are smooth. For dynamic cracks, it predicts that they accelerate to a limiting speed equal to the Rayleigh speed of the material [3], i.e. the speed of sound on a solid surface. However, experiment tells us that in a common fracture sequence in brittle materials, good examples being glasses and ceramics, an initially smooth and mirror-like fracturing face begins to appear misty and then evolves into a rough, hackelled region as the crack accelerates to a limiting velocity of about six-tenths the Rayleigh speed. Recently, researchers at the University of Texas have studied failure behaviour of very thin wafers of Plexiglas. The material is placed in a device that pulls it in opposite directions (mode-one loading) until a fracture develops at a prepared notch and the Plexiglas splits apart into two halves [5]. They have clearly shown that violent crack velocity oscillations occur beyond a speed of about one-third the Rayleigh speed, being correlated with the roughness of the crack surface. The origin of the divergence between theory and experiment suggests questions of microscopic impurities or imperfections in the material, experimental uncertainties or failure of theory. All of these features are unexplained using continuum theory.

We should remind ourselves that we have been discussing features of failure associated with rapid brittle fracture. Brittle fracture is certainly not the sole mechanism for materials failure when things are hit hard and fast; otherwise our world would be quite fragile. Basically there are two 'generic' classes describing materials failure; a material is brittle or it is ductile. In the first case, chemical bonds are broken and such a failure is easily recognized when you see glass shatter. For ductile failure, such a catastrophic event does not occur. 'Tough' materials like metals do not shatter; they bend because plastic deformation occurs by the motion of rows of atoms sliding past one another on preferred 'slip-planes' (dislocations) in contrast to bond breaking. This is why car fenders are not made of brittle materials like glass. These two general classes of failure do not depend on the 'details' of the interatomic interactions, but they do depend on the atomic packing of the three-dimensional solid [6]. Of course, the interatomic potential dictates the packing. But we also recognize that there are a limited number of atomic packings in nature. Glasses do not have extended crystallinity because atoms are packed randomly. They have no 'slip-planes' and no ductility. Glasses exhibit brittle failure. Crystals do not have the isotropy of glasses. In a certain sense one may view the crystalline solid as a defected solid because of the loss of perfect isotropy, the defect being multi-planar and infinite in extent! Because of the 'breaking' of the perfect isotropic symmetry, 'slip-planes' exist, dislocations are possible and ductility may win out over brittle failure. Face-centred cubic (FCC) packing is known to have a strong propensity toward ductility; body-centred cubic (BCC) much less so. We will encounter both modes of failure.

With the advent of scalable parallel computers, computational molecular dynamics is becoming a very powerful tool for providing immediate insights into the nature of fracture dynamics. Doing simulations and visualization at the Cornell Theory Center, we have developed methods and procedures for conducting such studies on the IBM RS/6000 Scalable POWERparallel Systems (SP) computer. It has become possible to perform an absolutely clean experiment of fracture with defect-free solids and we are coming up with some exciting results. Like the laboratory experiments, our initial interest was to study dynamic brittle failure [7]. We were able to follow the crack propagation over sufficient time and distance intervals so that a comparison with experiment became feasible. A detailed comparison between laboratory and computer experiments have shown commonality

in behaviour at the macroscopic scale. Using our ‘computational microscope’ we have discovered microscopic explanations for the limiting speed of the crack being significantly less than the theoretical limit. All of this has been achieved using simulations in two dimensions. We briefly summarize one simple but profoundly important point learnt in our studies to illustrate the work reported in this paper [8]. While the triangular solid is isotropic in the linear elastic regime, it is highly nonlinear and anisotropic near the cohesive limit, a feature that is not generally accounted for in fracture mechanics, or discussed in textbooks (figure 1). This is a consequence of the discrete nature of the atomic packing. We have found that there are two distinct directions in a 2D triangular LJ solid; a ‘stiff’ direction along which the yield strain is large and a ‘soft’ direction along which the yield strain is

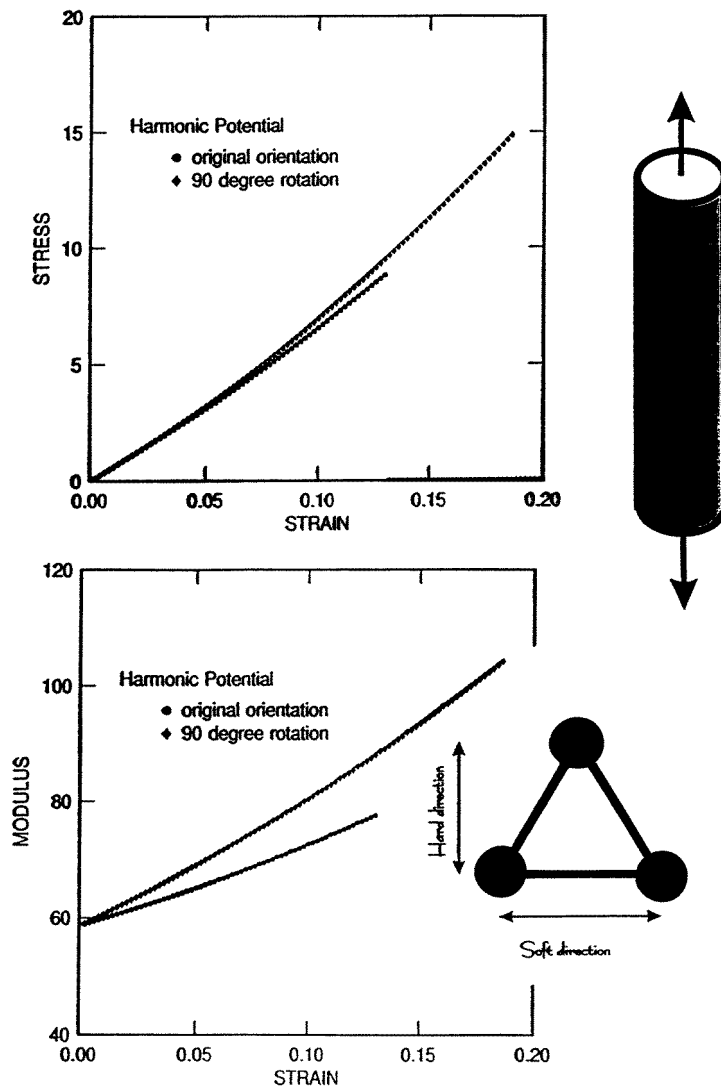


**Figure 1.** The elastic response of a two-dimensional triangular lattice of atoms couples to their nearest-neighbour atoms by Hookian springs which ‘break’ at a maximum extension.

smaller. A crack propagates more stably along the stiff direction because the bonds that are breaking lie in the soft direction. A crack moving in the stiff direction of a two-dimensional solid creates fracture surfaces of higher energy than those produced by a crack moving in the soft direction, despite the fact that the latter is breaking effectively stiffer bonds. In other words, the crack does not dynamically choose the low-energy cleavage direction as is generally supposed in conventional fracture theory. It is the detailed stresses near the crack tip, or hyperelasticity, rather than the surface energy that control directional stability of fracture and much more.

When going to three dimensions, we discover the dynamical instability in an FCC solid, but now the instability is immediately followed by an unexpected brittle-to-ductile transition, giving rise to a proliferation of loop dislocations and the arrestment of the crack [9, 10]. Given its low slip resistance, it is surprising that an FCC solid of rare-gas atoms could exhibit brittle failure at all. In order to explain our finding we show that the competition between bond breaking and interplanar slippage should be correlated with the behaviour of crystals near their cohesive limit (hyperelasticity). The FCC solid is also highly nonlinear and anisotropic near the cohesive limit and for certain directions breaking bonds, hence brittle failure, wins out over interplanar slippage and dislocation production or plasticity.

But first, let us discuss the tools that are needed for this study.

## 2. Modelling atomic solids and doing parallel computation

*What is discussed:* a brief introduction to the molecular dynamics method and parallel computation is presented. This discussion is not essential to the understanding of the following sections and may be skipped.

Our simulation tool is computational molecular dynamics and it is very easy to describe. Molecular dynamics predicts the motion of a given number of atoms governed by their mutual interatomic interaction and it requires the numerical integration of the equations of motion, force equals mass times acceleration or  $F = ma$  [11]. A simulation study is defined by a model created to incorporate the important features of the physical system of interest. These features may be external forces, initial conditions, boundary conditions and the choice of the interatomic force law. Our choice of simple interatomic force laws is dictated by our desire to investigate the ‘generic’ features of a particular many-body problem common to a large class of real physical systems and not governed by the particular complexities of a unique molecular interaction. Feynman summarized this viewpoint well on p 2 of volume 1 of *The Feynman Lectures in Physics*:

If in some cataclysm all scientific knowledge were to be destroyed and only one sentence passed on to the next generation of creatures, what statement would contain the most information in the fewest words? I believe it is the atomic hypothesis that all things are made of atoms—little particles that move around in perpetual motion, attracting each other when they are a little distance apart, but repelling upon being squeezed into one another. In that one sentence, you will see, there is an enormous amount of information about the world, if just a little imagination and thinking are applied.

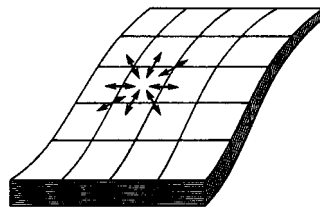
We choose to perform simulations with the simple rare-gas solid defining our *model material*†. The van der Waals bonding, giving the cohesion of the rare-gas solid, can be

† On p 73 of [1], Gordon comments on Griffith’s desire to have a simpler experimental material which would have an uncomplicated brittle fracture, he writes, ‘In those days models were all very well in the wind tunnel for aerodynamic experiments but, damn it, who ever heard of a model *material*?’

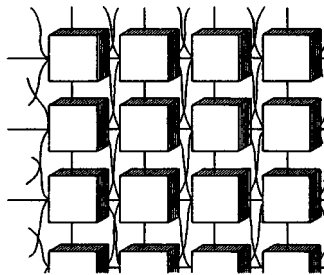
modelled accurately by the two-body Lennard-Jones potential, which served as a paradigm for studying classical many-body phenomena of atomistic systems in computational physics. Actually, it is no more difficult to use a potential that has directional forces (covalent or hydrogen bonding) or many-body forces. To list some, there are the Stillinger–Weber and Tersoff potentials for silicon, the embedded-atom potentials of Daw and Baskes for metals, the Barker many-body potentials for inert-gas solids, the Cole potentials for physical adsorption and many, many more [12]. We are using many of them and each has its own surprises! Because the rare-gas solid is known to be a ‘brittle’ material in two dimensions, we started with it; in three dimensions it is questionable.

A technical detail; we express quantities in terms of reduced units. Lengths are scaled by a parameter  $\sigma$ , the value of the interatomic separation for which the potential is zero and energies are scaled by the parameter  $\epsilon$ , the depth of the minimum of the potential. Simply speaking,  $\sigma$  is a measure of the size of the atom and  $\epsilon$  is a measure of how strongly the atoms bind to one another. The reduced temperature is  $kT/\epsilon$ .

Now a little about the computers we use. It was not much more than two decades ago that computational scientists were concerned that the speed of scientific computers could



‘Coarse-grain cells’ of a solid  
and nearest-neighbour interactions



Each processor models a cell  
with nearest-neighbour connections

- Each processor is responsible for a single physical region—all processors are identical.
- Nearest-neighbour interactions lead to very efficient nearest-neighbour communication.
- All processors should have essentially identical computational loads—‘load balancing’.

**Figure 2.** The important features associated with going from a physical problem to a parallel computer where physical space is subdivided into coarse-grained elements and each element is handled by a node of the parallel computer.

not go much beyond 4 Gigafllops, or 4 billion arithmetic operations per second and that this plateau would be reached by the year 2000! That is past history. With the concept of concurrent computing, a modern parallel computer is made up of several (tens, hundreds or thousands) small computers working simultaneously on different portions of the same problem and sharing information by 'communicating' with one another (see figure 2). The communication is done through 'message-passing' procedures.

The present record is over 1 Teraflops for optimized performance. However, before the commercial parallel computer came on the scene several researchers began building special purpose parallel computers in the early 1980s. One was the IBM Almaden SPARK computer for molecular dynamics [13]. In figure 3, we note the tremendous growth of the number of simulated atoms by molecular dynamics over the last three decades and the sharp increase in the 1990s with the appearance of large-scale parallel computers.

Parallel molecular dynamics is easy to implement efficiently in a message-passing environment. The key to the efficient algorithm is an efficient technique for handling the sums over particles which appear in the dynamical equations. If the summations over all  $N$  interacting particles had to be carried out for each of the  $N$  particles, we would have a problem with execution time scaling as  $N^2$ , a computational disaster for large systems.

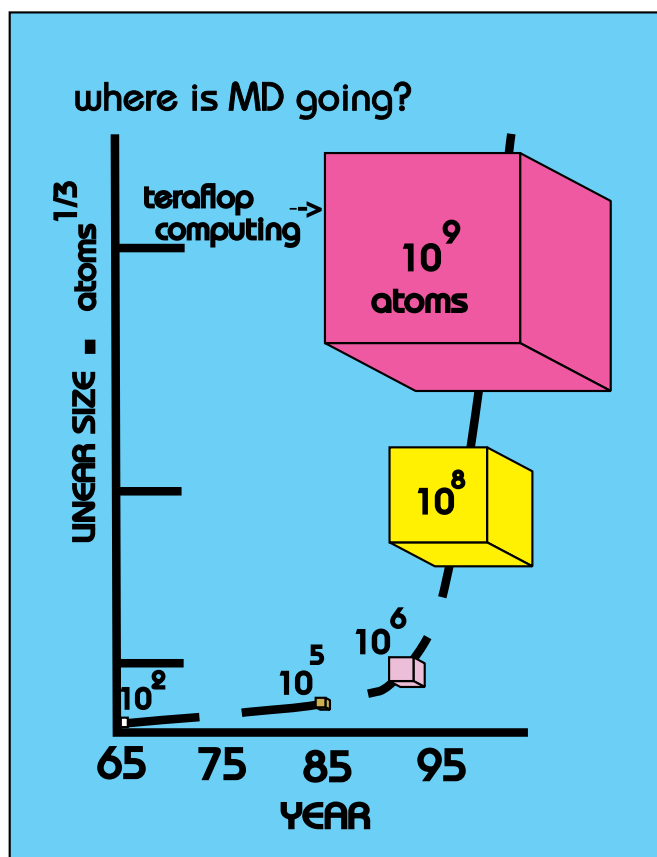
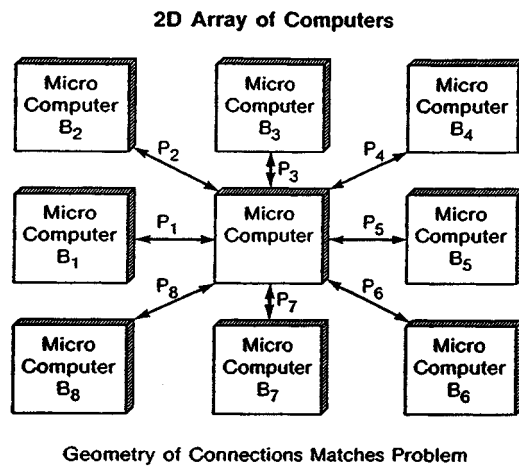


**Figure 3.** The historical growth of the total number of simulated atoms by molecular dynamics over more than three decades. Note the sharp increase in the 1990s because of the appearance of large-scale parallel computers.

However, if the forces are short range the problem may be reduced so that the execution time is proportional only to  $N$ . To do so, we restrict the summation to those particles with an interatomic separation that is less than the range of interaction by using coarse-grained tables and neighbour tables, both implemented with infrequent update [14, 15]. The computational space is divided up into coarse-grained cells which are chosen so that in searching for the neighbours of a given atom, only the coarse-grained cell in which it is located and the nearest-neighbour and next-nearest neighbour cells need to be considered. Since placing the particles in the proper cells can be done in linear time, we have reduced the problem from one which scales as  $N^2$  to one which scales with  $N$ . With a parallel computer with the number of processors increasing with the number of coarse-grained cells (the number of atoms per cell remaining constant), the computational burden remains constant. The task of computing the forces and updating the positions of the particles in a given cell is given to a processor of the parallel computer. To perform this task, the processor will first have to learn



- Parallel computation algorithm
1. Coordinate communication phase
    - For each communication path  $P_i$   $i = 1;8/$  each computer
      - transmits coordinates of its atoms along  $P_i$
      - receives coordinates along opposite path
  2. Force accumulation phase
    - For each particle in computer's own space,  $B_0$ 
      - Computes force from neighbours in  $B_0$  and  $B_i$
      - Neighbour tables can be used to limit the number of force calculations required
  3. Integration phase
    - For each particle in computer's own space,  $B_0$ 
      - Update the positions and momenta
  4. Global computation phase
    - Collect and sum partial kinetic energy terms
    - Pass total kinetic energy to each computer
    - Renormalize velocities
  5. Final phase
    - Once every 10–100 time steps
      - Update the neighbour tables
      - Move the particles to a new computer if they have crossed the coarse-grained cell boundaries

**Figure 4.** The parallel computation algorithm for molecular dynamics. In the 2D array shown, the geometry of connections matches the problem [11].

$$S(\text{speedup}) \equiv \frac{\text{execution time for one processor}}{\text{execution time for 'p' processors}}$$

Ware's *Two-State* Model

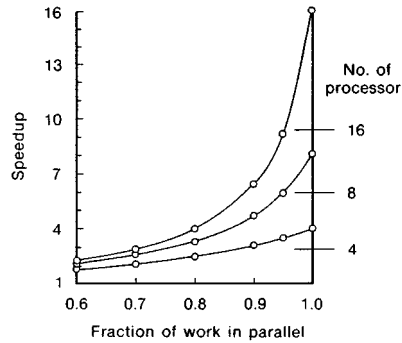
Binary Machine or  $\begin{cases} \text{all 'p' processors operating} \\ \text{only one processor operating} \end{cases}$

$f_i \equiv$  fraction of work processed in parallel

$$S(f_i; p) = \frac{1}{(1 - f_i) + f_i p}$$

$f_i = 1$ ;  $S = p$  parallel

$f_i = 0$ ;  $S = 1$  'not' parallel



Speedup as a function of parallelism and number of processors

**Figure 5.** The speed-up for parallel processing for a single application based on the very simple Ware model. The inset shows speed-up as a function of parallelism and number of processors. This really 'tells' the story!

the positions of neighbouring particles. Thus we are led to divide the parallel algorithm into a communication phase followed by a computation phase. Efficiency demands that the communication bandwidth grows linearly with the number of processors. This can be achieved by connecting the processors with a network that allows the communication to be done in parallel. In figure 4, details of the parallel computation for molecular dynamics is outlined.

The perfectly efficient parallel computer would exhibit linear speedup: the computation rate of  $P$  processors would be  $P$  times that of a single processor. However, communication and other global demands may dominate if a sufficiently fine-grained parallel structure is defined. If we identify the single processor operation as an overhead step, we see that speed-up depends in a sensitive way on the fraction of work done in parallel; if a large proportion of the effort goes into overhead, the efficiency for the parallel computer drops dramatically (figure 5). For another description of fast parallel algorithms for molecular dynamics with short-range forces, we refer the reader to Plimpton's article [16].

### 3. Computer experiments for two dimensions

*What is shown:* laboratory findings occur in our simulation, essentially 'validating' our simulations concerning their relevance to 'real-world' fracture phenomena. But most importantly, we see a dynamic instability of the crack tip for a perfect (defect-free) atomic system. We can only conclude that this fracture behaviour is universal, its origin is in the dynamics and is not material related. We also show that it is the elasticity at breaking (hyperelasticity) that governs the fracture behaviour.



Why do we refer to ‘experiments’ in the title of this section? In a certain sense, one can view the simulation methodology as giving experimental information from a model, idealized universe. This approach has a mixture of theory and experiment and it has been labelled a ‘third kind of science’. By computationally solving the theoretical models in detail, a wealth of information about a physical phenomenon is produced that can be viewed as experimental data. Like any other experimentalist, we have to ask the right questions and have to measure the right things.

Our early interest was to study the brittle fracture of an idealized two-dimensional solid [7] by following the crack propagation over sufficient time and distance intervals so that a comparison with experiment became feasible. The system size was as large as  $2 \times 10^6$  atoms. Why  $10^6$  atoms? A 2D wafer of  $10^6$  atoms has 1000 atoms on each side, which we found to be large enough to simulate the early stages of fracture dynamics. The slab length was long enough for the crack to reach its maximum speed before the elastic stress waves produced by the advancing fracture reflected off the wafer’s edges and returned to the fracture point. Size demands more atoms and more atoms demand more computing, not only because of the increased size but also because the natural time scale expands; that is, it takes more time for the crack to traverse the system. The following simulations revealed a very rich dynamics in the failure process.

The slab is initialized at a very low temperature, a notch of specified size is cut midway in the lower horizontal slab boundary and an outward strain rate  $\dot{\epsilon}_x$  is imposed on the outermost columns of atoms defining the opposing vertical faces of the slab. A linear velocity gradient is established across the slab and an increasing lateral strain occurs in the solid slab. At a sufficiently large strain, depending upon the choice of notch length and other things, the crack begins to move from the notch tip. At the onset of crack motion, the imposed strain rate is held constant or is set to zero and the simulation is continued until the growing crack has traversed the total length of the slab.

### 3.1. The crack’s dynamical instability

Figures 6 and 7 summarize graphically the important findings of a typical 2D fracture simulation. In figure 6, we see that the brittle crack initially propagates in a straight line and leaves ‘mirror’ cleaved surfaces. At the onset of the instability (second image), the crack begins to roughen and then to oscillate back and forth (third image) achieving a forward speed equal to 0.57 of the Rayleigh speed  $c_R$ . For speeds less than  $0.32c_R$ , the acceleration of the crack tip is quite smooth; however, the ‘instantaneous’ tip speed is very erratic after reaching a speed of  $0.32c_R$ . All of these features are in agreement with the laboratory findings of Fineberg *et al* [5]. In figure 7, we see objects appearing as slanted, inverted Vs being emitted from the moving crack tip, first to the right then to the left. The Vs are simply acoustic wakes created by moving dislocations that are travelling away from the crack at  $30^\circ$  to the vertical. These dislocations are initiated with a change of crack direction in the zig-zag motion and travel at approximately the speed of sound for the bulk solid. They may be traced back to their origin by constructing an imaginary line  $30^\circ$  from the vertical and passing through the V. The vertical separation between neighbouring dislocations equals the wavelength of the oscillating crack. These dislocations provide an excellent signature for crack oscillation. Like the laboratory experiment, the influence of physical boundaries is a concern when sound and dynamical defects reflect from them. It should be noted that the onset of the instability relative to tip motion occurs significantly earlier than it takes sound to travel from the tip to a lateral boundary and return.

Another class of dislocations exists which are not apparent in the grey-scale pictures of

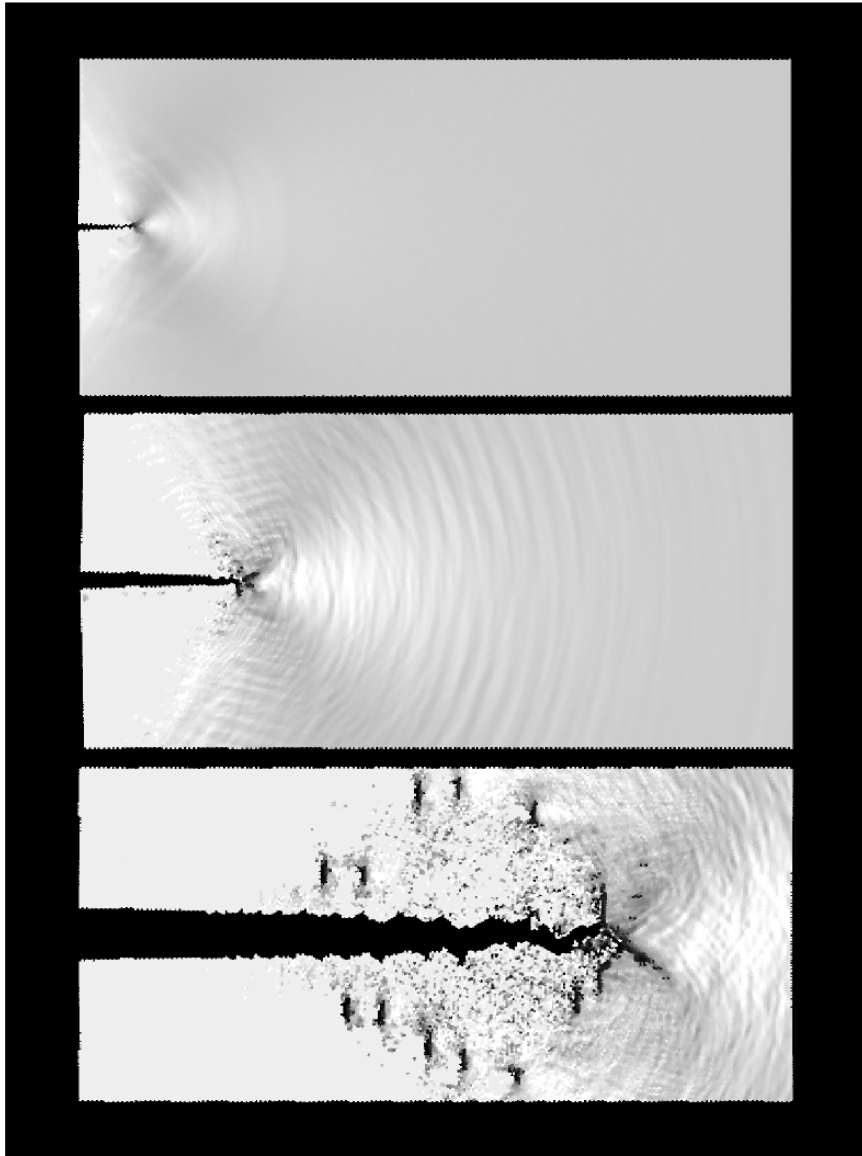


**Figure 6.** This figure shows near-field views of the propagating crack at three different times: for an early time when its speed is less than one-third of the Rayleigh speed  $c_R$  and the crack surface is smooth; at the time when its speed is around one-third of the Rayleigh speed  $c_R$  and the crack surface is beginning to roughen; for a late time when the crack's forward speed is constant, equal to one-sixth of the Rayleigh speed  $c_R$ , and the crack surface is very rough, being created by a zig-zag motion.

the transverse velocity fields as presented in figure 7, but appear as dark vertical 'dashes' in the late-time snapshot in figure 6. In figure 8, dislocation locations are shown at various times during fracture tip motion as blue dots, where a dislocation is identified as an atom with a fivefold coordination (hence we also see blue dots at the fracture surface). We find the appearance of an abundance of dislocations being emitted near the crack at right angles

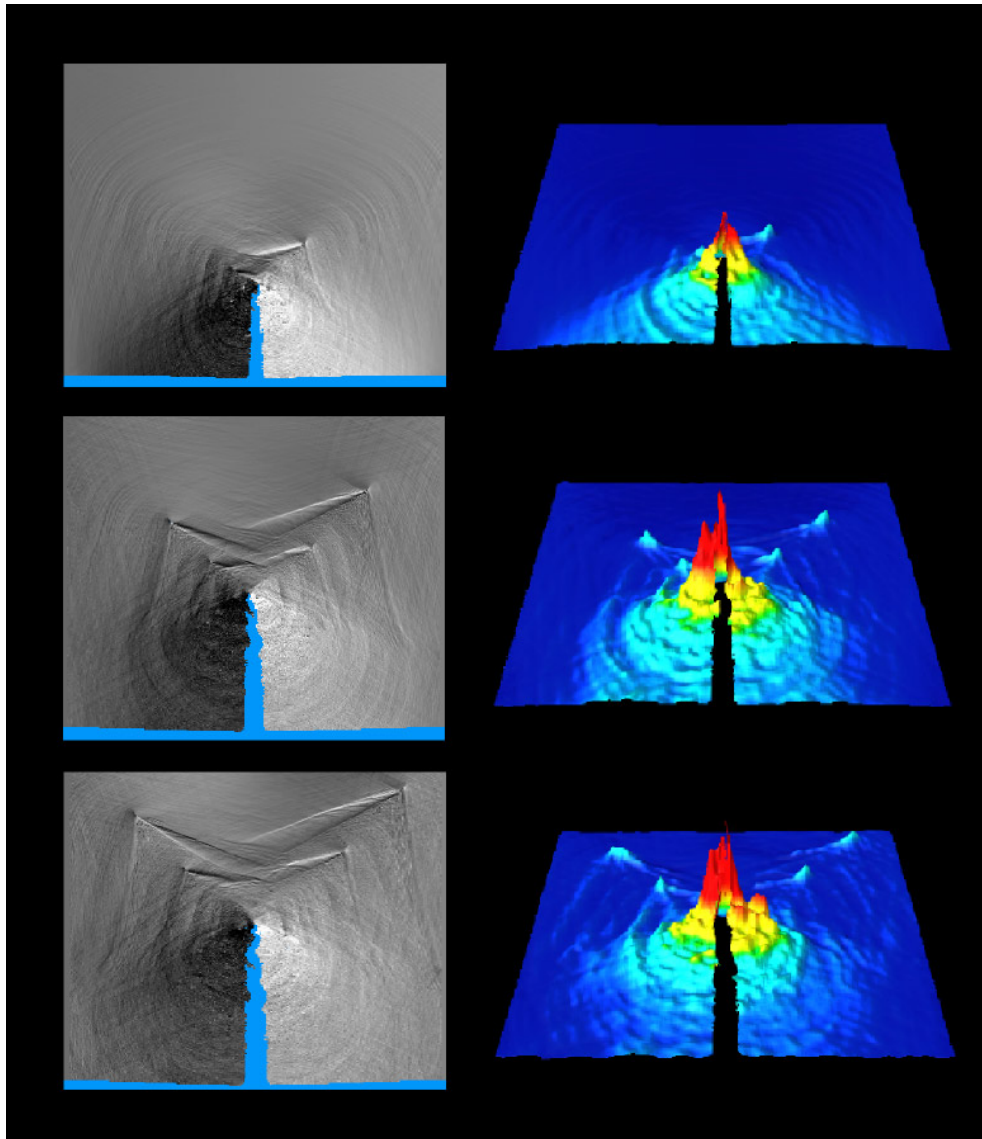


**Figure 7.** This figure shows far-field views of the propagating crack. The left-hand column shows the time evolution of the propagating crack using a grey-scale rendering of the instantaneous local velocity, going from dark grey for the most negative velocity to light grey for the most positive velocity. The right-hand column shows the respective frames coloured by temperature, red being hot and blue being cold.

from the forward motion! By examination, we observe that the transverse dislocations go out some distance, then return to the fracture surface where they disappear. The spacings between these dislocations are quite regular. We can understand their origin as a transverse slippage between two neighbouring rows of atoms arising from a growing shear stress at the crack tip as the ever-increasing cascade of broken bonds in the forward direction allows ever increasing severed rows of atoms to want to relax laterally. This build-up of severed atomic

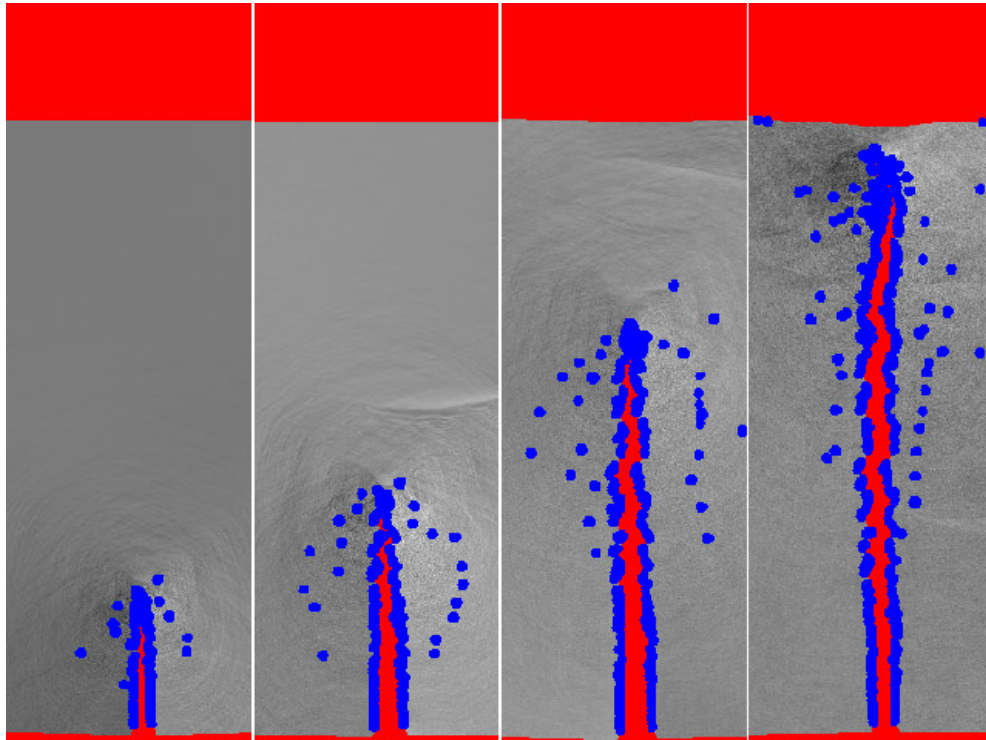


**Figure 8.** Snapshot pictures of the dislocations emitted from a travelling crack. They are denoted by blue dots for atoms with a fivefold coordination. The time sequence goes from left to right.

rows will eventually be sufficiently large enough to overcome the barrier to slippage. The front to slippage will manifest itself as a dislocation. Of course this is a repeating process, hence there is a continual creation of transverse dislocations. Also, the return of dislocations to the crack surface and the healing of the surface is a consequence of neighbouring bands of matter bounded by slip planes relaxing to equilibrium.

To highlight the microscopic features of the crack dynamics, we present figure 9 which is a short-time interval sequence of close-up views of the crack tip at an early time and at a late time. The onset of the crack instability begins as a roughening of the created surfaces which eventually results in the pronounced zig-zag tip motion; i.e. ‘smooth  $\rightarrow$  rough  $\rightarrow$  zig-zag’ corresponds to ‘mirror  $\rightarrow$  mist  $\rightarrow$  hackle’. The roughening occurs before dislocation emission and corresponds to a point in the crack-tip dynamics where the time it takes the tip to traverse one lattice constant approximately equals the period for one atomic vibration. Hence, the bond-breaking process no longer sees a symmetric environment due to thermal averaging, but begins to see local atom configurations ‘instantaneously’ distorted from perfect lattice symmetry. This gives rise to small-scale (atomic) fluctuations in the bond-breaking path and hence, atomic roughening. This roughening could trigger larger-scale deviations if the dynamics is intrinsically unstable. In the hackle region, the growth of the fracture is not simply a sharp one-dimensional cleavage progressing in a zig-zag manner at  $30^\circ$  from the mean crack direction. Instead, we see a staircase growth of connected ‘ideal  $30^\circ$  segments’, resulting in a net forward angle of less than  $30^\circ$  from the horizontal before changing the local direction by  $\sim 60^\circ$ . The ‘ideal  $30^\circ$  crack segments’ open at a velocity

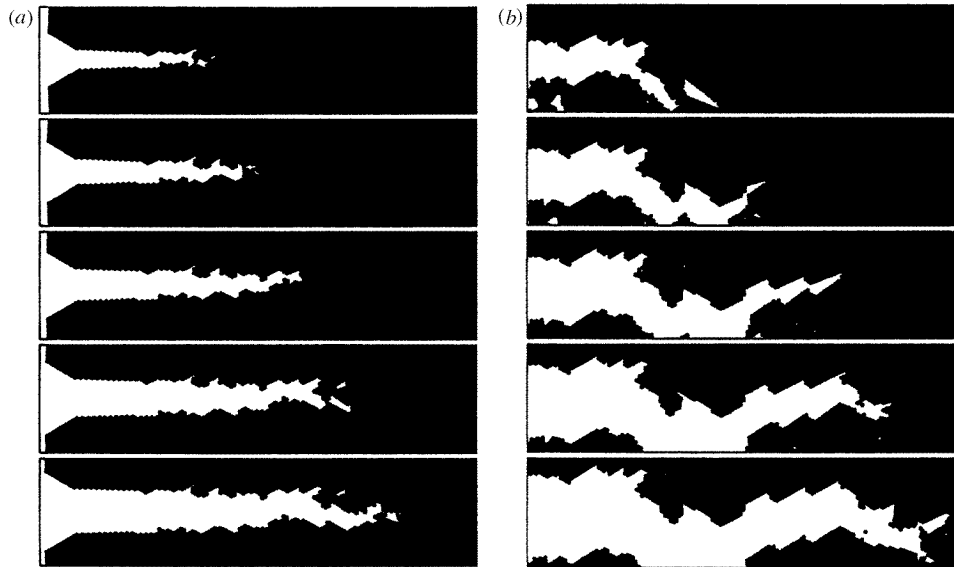


**Figure 9.** (a) The onset of crack instability, where roughening of the crack surface begins to appear; (b) late-time zig-zag crack propagation.

approximately equal to the Rayleigh speed  $c_R$ . The origin of the erratic velocity oscillations is associated with the staircase branching and the connecting of regions of failure at the crack tip. The oscillating zig-zag motion of the crack tip and the segmented staircase growth contribute to the ‘apparent forward’ crack speed being six-tenths of the theoretical prediction.

Figure 10 shows a contour plot of the dynamic crack-tip stress  $\sigma_{\theta\theta}$  in a region spanning the crack tip [17]. The white line at the bottom of the figure gives the silhouette of the crack profile. As the crack tip accelerates, the stress field flattens in the forward direction and expands laterally. Crack roughening occurs at approximately the time when the stress distribution around the forward direction is flat, albeit noisy. With the disappearance of the prominent forward peak in the stress field, the crack can fluctuate off centre and the perfect forward motion is destroyed. By the time the crack tip has achieved its prominent zig-zag wandering the stress field is very broad and distorted, consistent with the erratic motion.

The effect of initial crack length is also examined. The initial notch lengths,  $a_i$  are 10, 20 and 40 atomic spacings. The crack extension  $\Delta a$ , versus time  $t$ , curves for the three cases are shown in figure 11, where  $\Delta a$  is the difference between the current and initial crack tip positions. The critical tensions for crack initiation,  $T_c$ , are related to the initial crack lengths by the relation  $T_c \sqrt{a_i} = \text{constant}$ . The longer the initial crack is, the lower the critical tension needed and the sooner the crack growth starts. Thus the relation between the crack initiation time  $t_i$ , and the initial crack length is  $t_i \sqrt{a_i} = \text{constant}$ . This is in agreement with elasticity theory. We have learned that the crack accelerates smoothly to a speed around one-third of the Rayleigh wave speed and then starts to create rough surfaces. The critical velocities are  $0.32c_R$ ,  $0.34c_R$  and  $0.31c_R$  for the cases with initial crack lengths being 10, 20 and 40 atomic spacings, respectively. Dislocations appear at a later time. The dynamics of the smooth growth can also be scaled by  $\sqrt{a_i}$ . The onset time can be related by  $(t_R - t_i)/\sqrt{a_i} = \text{constant}$  for roughening and  $(t_D - t_i)/\sqrt{a_i} = \text{constant}$  for dislocation emission. In figure 11(b), the curves of the scaled crack extension,  $\Delta a/(a_i)^{0.33}$ ,

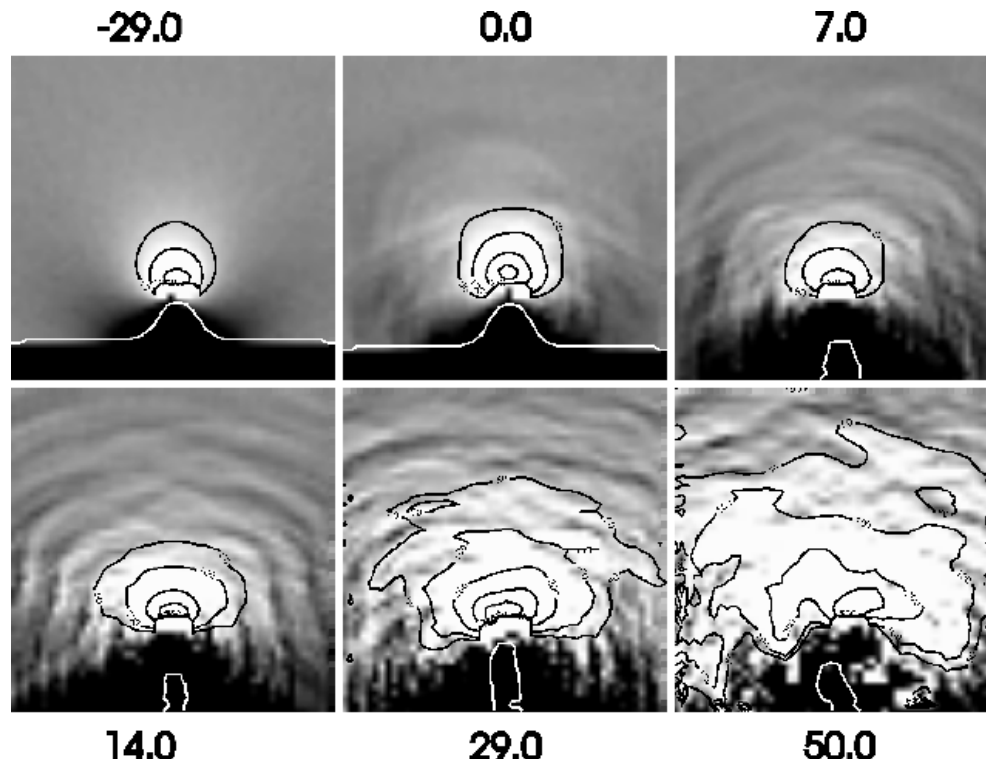


**Figure 10.** Contour plot of the dynamic crack-tip stress  $\sigma_{\theta\theta}$  in a region of the crack tip for various times.

versus the scaled crack growth time,  $(t - t_i)/\sqrt{a_i}$ , are plotted and the onset times for roughening and dislocation emission are marked. Notice that the three curves collapse together until the occurrence of the dislocations, a very important finding in dynamical scale invariance.

### 3.2. Crack branching and anisotropic hyperelasticity

In the early molecular dynamics simulations, the crack notch was directed not in the ‘cleavage line’ of the triangular lattice, or the lowest-energy surface path; conventional wisdom associates the lowest-energy surface as the favoured cleavage direction. In figure 12, we show again a time sequence of the crack moving in the ‘non-cleavage’ direction. We also show a similar simulation, but with the crack oriented in the ‘cleavage’ direction. Look what happens to the cleavage crack! This crack does not proceed along this cleavage line, but turns  $30^\circ$  from the cleavage direction. Because of the hexagonal crystal symmetry, this branched direction corresponds to an equivalent ‘non-cleavage’ direction. We realized that elastic nonlinear anisotropy (like figure 1) leads to significantly different failure strains for the two different symmetry directions and that this is the explanation for the branching feature [8]. This is consistent with the picture that the crack’s dynamics is governed by the anisotropic mean-field elasticity associated with large strains.

The bulk elastic modulus is profoundly anisotropic for large strains. In figure 13, we present the Young’s modulus as a function of tensile strain for a 2D LJ lattice for two

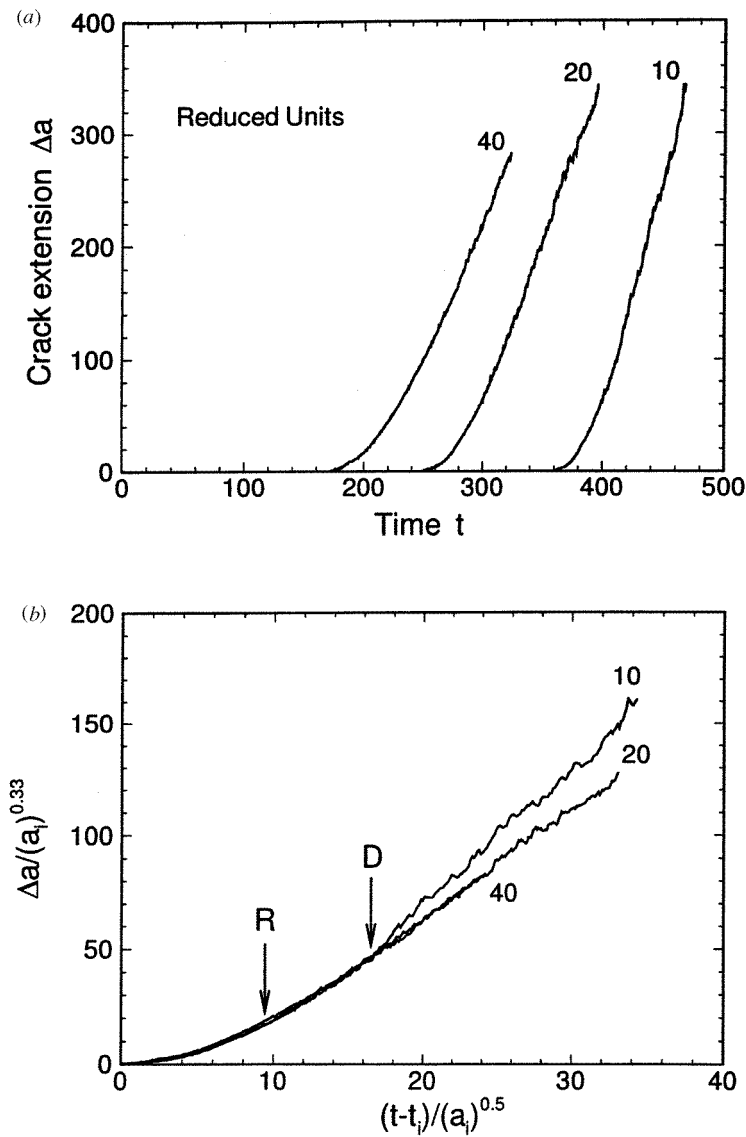


**Figure 11.** (a) The crack extension  $\Delta a$ , versus time  $t$ , curves for the cases with initial crack lengths of 10, 20 and 40 atomic spacings. (b) The scaled crack extension versus scaled time curves for the cases with initial crack lengths of 10, 20 and 40 atomic spacings.

orthogonal directions. In what we term the ‘soft’ direction, the atoms are an equilibrium spacing apart, while in the ‘stiff’ direction the spacing between rows of atoms is  $\sqrt{3}/2$  of the lattice constant. We used this terminology in figure 1. The soft direction corresponds to the cleavage direction, and the stiff direction is the non-cleavage direction. We see that lattice properties under large deformations are not isotropic. At large strains, the smallest Young’s modulus is in the soft direction and the largest in the stiff direction. We also note that the soft direction is the weak direction, failing at a strain of  $\sim 13\%$

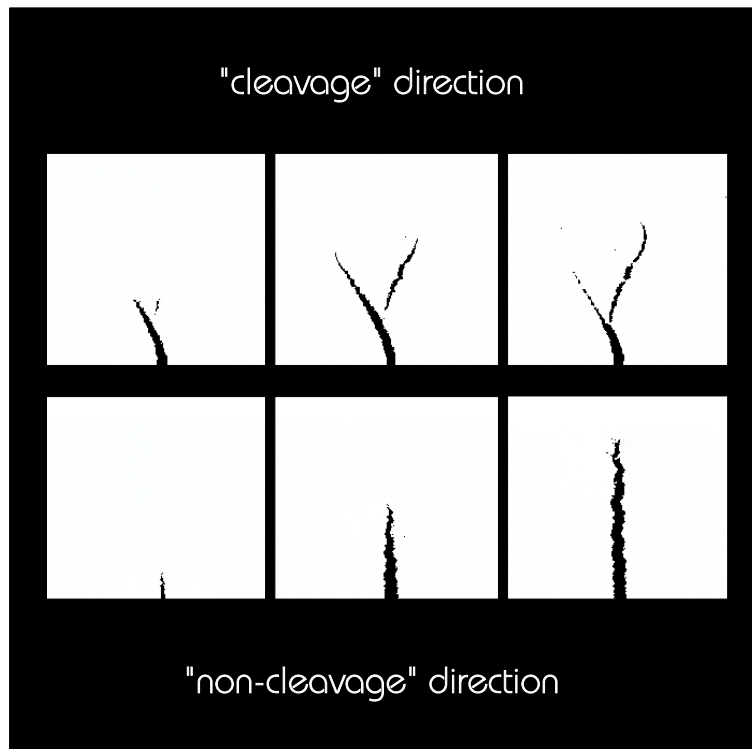


**Figure 12.** Black/white rendering of the time evolution of the propagating crack. The time sequence goes from left to right. The top row is for the crack initially moving in the ‘cleavage’ (soft) direction and the bottom row is for the crack initially moving in the ‘non-cleavage’ (stiff) direction.

in contrast to the stiff direction that is the strong direction that has a failing strain of  $\sim 19\%$ . The elastic nonlinearity leading to significantly different failure strains for the two different symmetry directions is the explanation for the branching feature, suggesting a simple picture for the crack-path behaviour; the crack path follows the stiff direction because the transverse bond breaking direction is then soft and fails at a much lower strain. This occurs at high crack velocities where the strain field has broadened about the forward direction (figure 10). If the crack is initially moving in the stiff direction, it will ‘stay’ in that direction. Otherwise, a crack initialized in the soft direction will eventually ‘branch’ by  $\pm 30^\circ$ , the branch can be a single crack or a multi-crack with a vertex at the point of branching. If the branch is a single crack, the material will ‘tear’ in the symmetrically opposite side because of the created mixed mode (mode I and mode II) asymmetry.

Multimedia versions of our 2D atomistic simulation studies of fracture are available via the World Wide Web: 2D fracture: <http://www.almaden.ibm.com/vis/fracture/prl.html>

Let us now consider three dimensions.



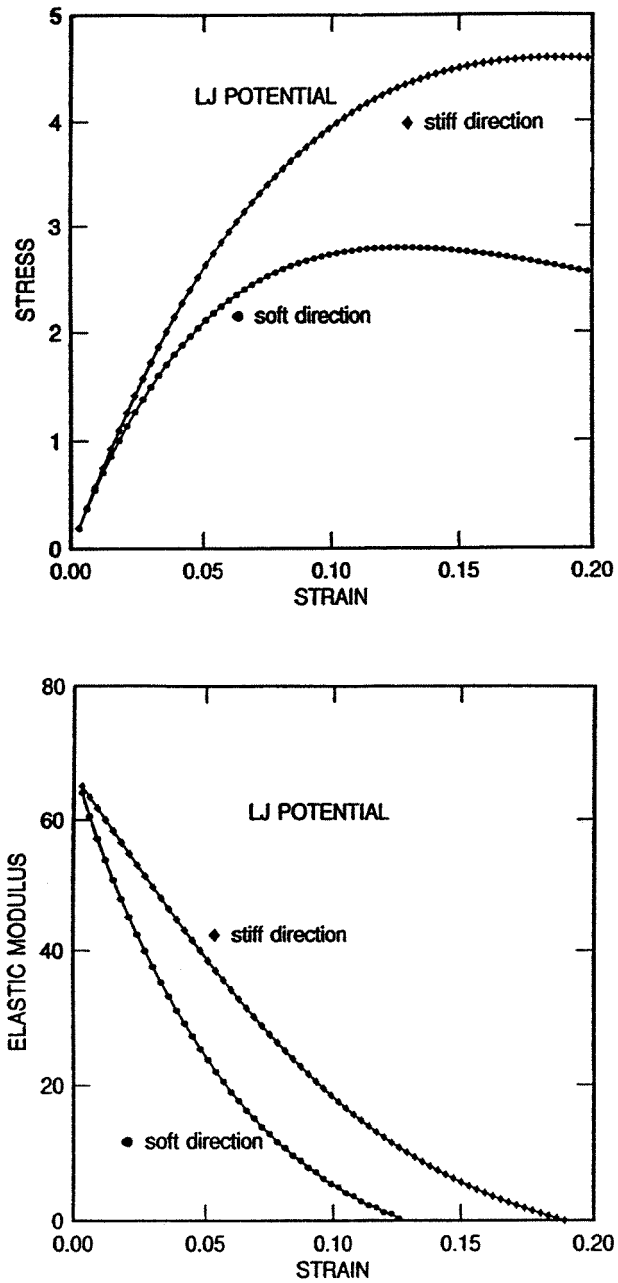


Figure 13. Dependence of Young's modulus on tensile strain for a 2D LJ crystal.

#### 4. Computer experiments for three dimensions

*What is shown:* we find that an FCC solid (e.g. xenon, copper) may begin failing by brittle cleavage. When the crack velocity approaches one-third of the Rayleigh sound speed, a 'dynamic brittle-to-ductile' transition occurs. This supports the thesis that the dynamic

instability is a general feature of rapid brittle fracture. Hyperelasticity determines whether an FCC solid fails initially by brittle fracture or plastic failure.

We choose to continue our fracture studies with the simple rare-gas solids described by the simple Lennard-Jones potential defining our ‘model’ material. This is similar, in spirit, to Griffith’s choice of glass as a ‘model’ material for the study of fracture, so as to simplify the phenomenon by using the ‘simplest’ material. However, Griffith knew that glass is brittle. Such is not the case for the rare-gas solid. Kelly and Macmillian [6] state in their classic text *Strong Solids*, ‘At liquid hydrogen temperature, . . . imperfect crystals of krypton have about the hardness of butter on a cold day’. Theoretical studies suggest that the rare-gas solids, as well as most FCC solids, exhibit ductility inherently. We will show that a classical rare-gas crystal at zero temperature can fracture in a brittle fashion.

We give some important details of the simulation. The atomic system is a three-dimensional slab with a planar notch and having a total of 100 509 696 atoms. Figure 14 shows a picture of the simulated solid system. We show only those atoms that have a cohesive energy less than 97% of the ideal bulk value. This reduces the number of atoms seen by approximately two orders of magnitude in three dimensions; the visible atoms are associated with faces of the slab and initial notch, surfaces created by crack motion, local interplanar separation associated with the material’s dynamic failure at the tip and topological defects created in the otherwise perfect crystal. Otherwise, to make a movie with 400 configurations by storing the positions and velocities of  $10^8$  atoms for each configuration would require handling 680 Gigabytes of data, the equivalent of the stored information in

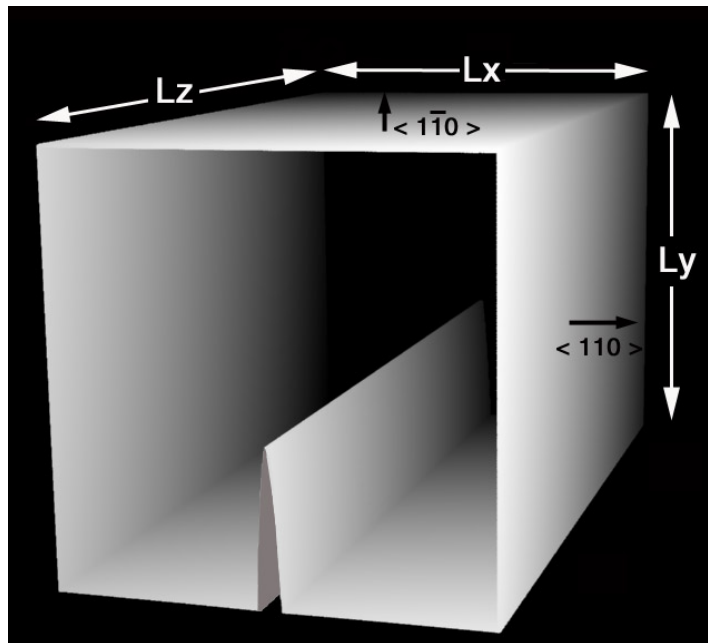


**Figure 14.** The notched rare-gas solid showing the coordinate system adopted for the simulation, the lengths of the solid’s orthogonal sides, and the FCC crystal orientation. The picture shows a ‘transparent’ solid except for the exterior faces and the surface of the notch. Because of periodic boundary conditions, the front and back faces are not exterior surfaces and are therefore transparent.

printed texts in a modern library (see figure 15). The clock-time for a  $10^8$  atom simulation is  $2\frac{1}{2}$  days on an 512-node SP parallel computer, or 30 000 CPU hours of computer total time. A ‘real’ crack would traverse a laboratory nanocrystal in approximately a nanosecond.

The exposed notch faces are in the  $y$ - $z$  planes with (110) faces, and the notch is pointed in the  $[1\bar{1}0]$  direction. We note that the (110) face does not have the lowest surface energy; i.e. the (111) surface would be taken as the cleavage plane for brittle fracture. Our choice of the (110) surface is based on the hyperelastic anisotropy of the FCC packing which will be discussed in detail in a short while. The slab is initialized at zero temperature and an outward strain rate  $\dot{\epsilon}_x$  is imposed on the outermost columns of atoms defining the opposing vertical faces of the slab. A linear velocity gradient is established across the slab and an

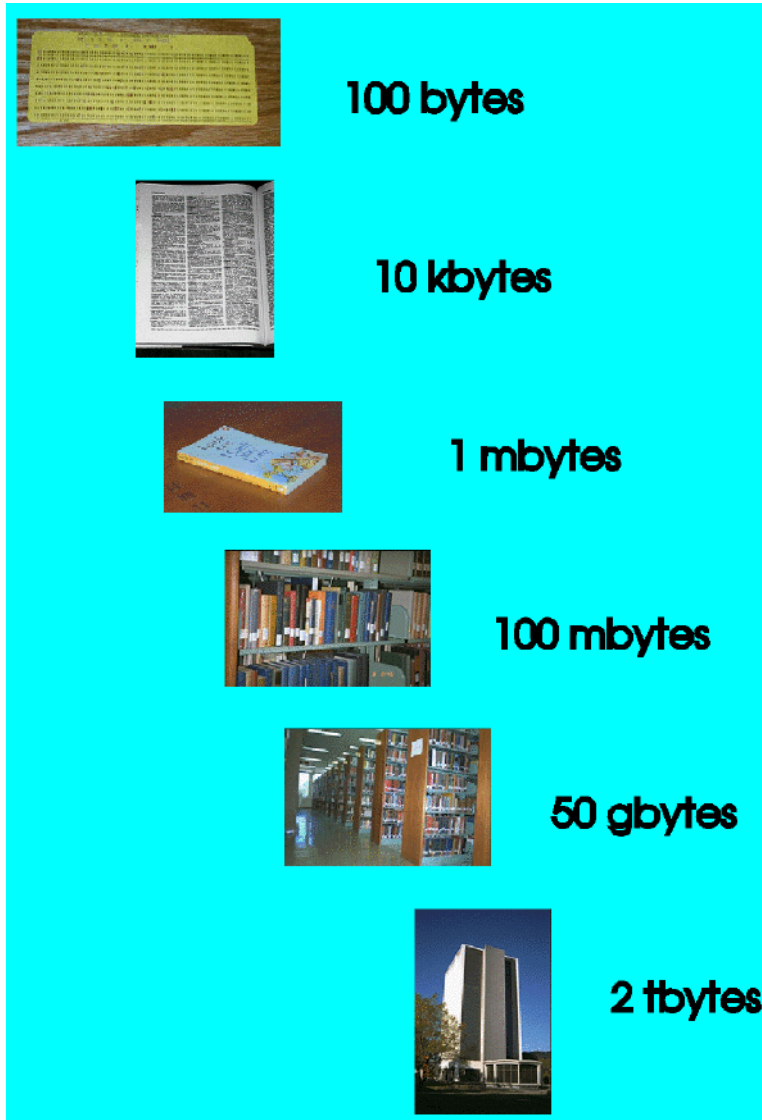


**Figure 15.** Data content in ‘various storage devices’.

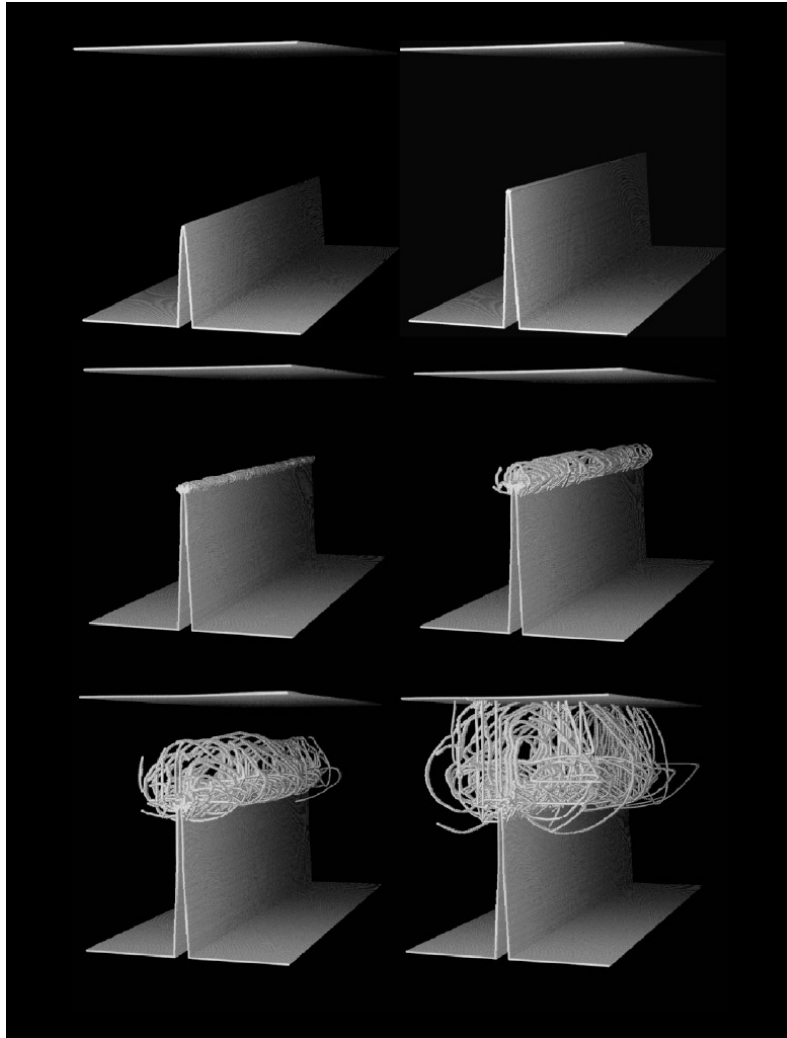


**Figure 16.** Temporal sequence of the crack dynamics in a  $10^8$  atom slab (ordered from left-to-right and top-to-bottom) is shown as landscapes of the crack surface growing due to brittle fracture (the first two images for times 1, 32), the initiation of the instability (time 43) and the subsequent growth of dislocations (the last three images are for times 52, 68, 90) after the transition to ductility. Only atoms with cohesive energy less than 97% of the bulk value are displayed, resulting in the selected visualization of atoms neighbouring surfaces and dislocations. The slab's top and bottom exterior surfaces are included.

increasing lateral strain with time occurs in the solid slab. The solid fails at the notch tip when the solid has been stretched by  $\sim 1.5\%$ . We adopt the initiation of crack tip motion as zero time. The imposed rate is set to zero at  $\delta T_s$  time beyond motion. We will be referring to time in 'reduced time units'. For our rare-gas solids, one reduced time unit is equal to 2 ps.

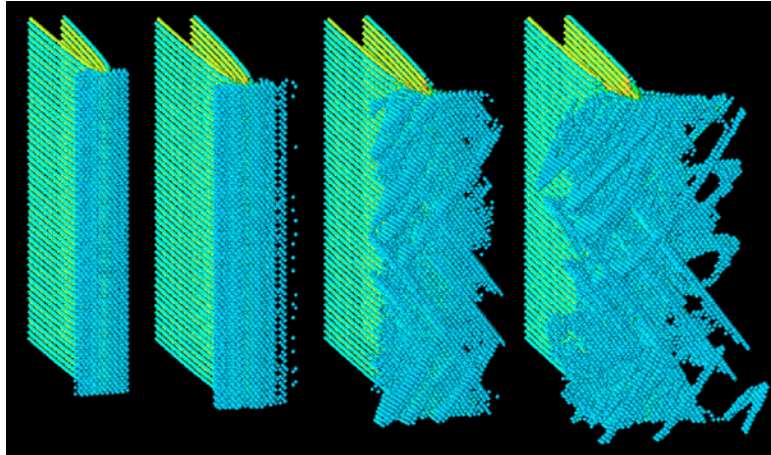


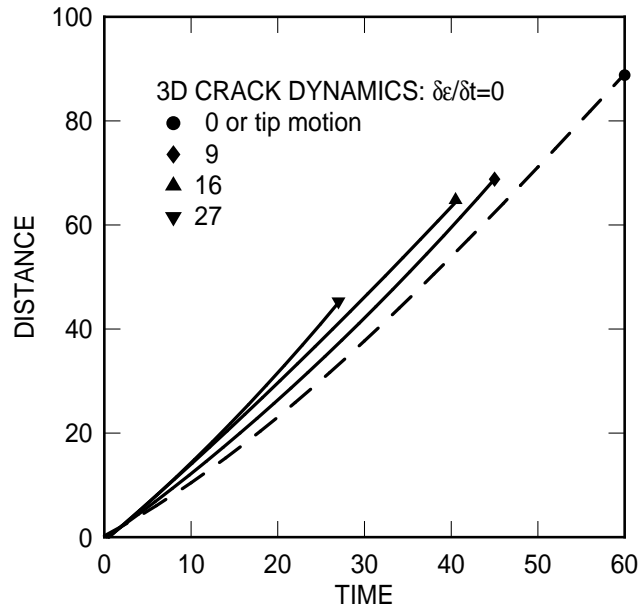
**Figure 17.** Magnified off-diagonal perspective views of the process zone during the time period of the brittle-to-ductile transition (at times 36, 43, 49 and 54). The colouring is according to the potential energy of the atom, the dislocations appearing as cyan and the surfaces as blue and yellow.

#### 4.1. The ‘brittle-to-ductile’ transition

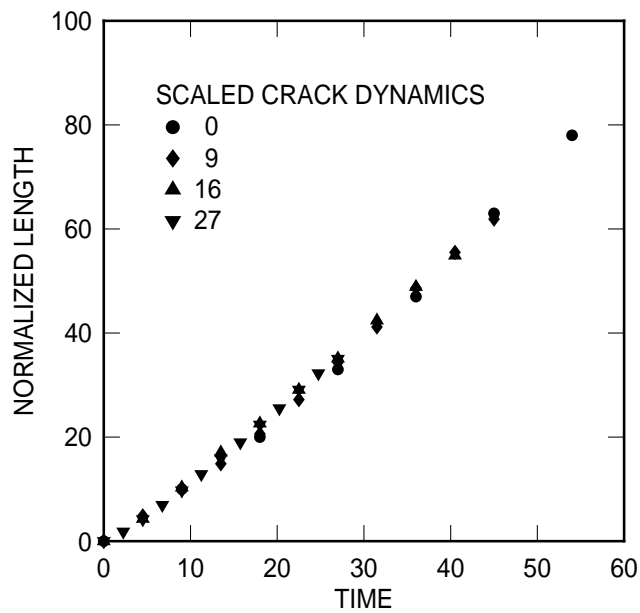
Figure 16 shows our simulation of the  $10^8$  atom slab and  $\delta T_s = 16$  (reduced time), where the dynamic ‘brittle-to-ductile’ transition was discovered and observed to occur at  $\delta T_t = 43$  [10]. In the time interval 0 to 42, the crack motion is representative of brittle fracture, with planar cleavage of the bonds between the two (110) neighbouring atomic sheets defined by the initial notch. The small bud at the crack tip represents local expansion and we refer to this region as the ‘process zone’. During brittle fracture, this process zone represents no plasticity, but at a time of 43 the bud begins to blossom into a ‘flower of loop dislocations’. The crack slows to a stop and continues to dissipate elastic energy through the continued creation and motion of dislocations. Hence, a *dynamic* brittle-to-ductile (B–D) transition occurs in the fracturing of this rare-gas nanocrystal.

Figure 17 shows magnified off-diagonal perspective views of the process zone during the time period of the brittle-to-ductile transition. We note that just prior to the B–D transition, the process zone is symmetric. The zone then becomes asymmetric and rapidly broadens into a wall of embryonic dislocations. The crack surface had begun to roughen prior to dislocation emission. In our two-dimensional fracture simulations, we saw a similar roughening which was identified as the onset of an intrinsic dynamical instability of the brittle fracture process. For the three-dimensional simulation, this roughening extends in depth as a one-dimensional step which is a few atom diameters wide. However, the three-dimensional B–D fracture transition immediately follows, in sharp contrast to the fracture of the two-dimensional rare-gas films where brittle fracture prevails. Furthermore, the surface roughening (i.e. the brittle instability dynamics) occurs when the crack tip velocity equals  $\sim 0.36$  of the Rayleigh speed of sound for the rare-gas solid, similar to what we found in the two-dimensional systems.

For comparison with experiment, we refer the reader to the transmission electron micrograph of an arrested crack in silicon above the ductile transition temperature [18], where very similar dislocation activity is visible in the presence of the silicon crack tip. However, unlike our experiment, it was not possible to determine the dynamic origin of these dislocations.



**Figure 18.** The crack-tip distance versus reduced time is presented for various times  $\delta T_s$  where the strain rate is set equal to zero.



**Figure 19.** The crack-tip distance in figure 18 is scaled by the square root of enhanced strain  $\delta\epsilon$  beyond  $\delta T_s = 0$ ;  $\delta\epsilon = 1.2, 1.35, 1.6$  for  $\delta T_s = 9, 16, 27$ .

In hopes of establishing a relationship between the brittle fracture dynamics and the brittle-to-ductile transition [9], we investigated the dynamic histories of the crack motion

up to the time for the transition  $\delta T_t$  for different choices for  $\delta T_s$ . In figure 18, we present the crack-tip distance versus time for the various times where the strain rate is set equal to zero. We find that the later the strain rate is set equal to zero, the earlier in the dynamics is the point at which the brittle fracture crosses over to ductile failure;  $\delta T_t = 45, 40, 27$  for  $\delta T_s = 9, 16, 27$ . Only for  $\delta T_s = 0$  do we observe that a brittle crack propagates throughout the entire length of the solid. A primary interest is to find a dynamical feature at the transition point that is common to all of the simulations. Such a feature was found in our 2D simulations, where the speed for the onset of the brittle fracture instability was  $\sim 33\%$  of the Rayleigh speed. In 3D, we now find that the transition from brittle fracture to plastic failure occurs when the tip speed  $v_t$  equals 0.36 of the Rayleigh sound speed  $c_R$ .

This supports the following scenario for the dynamic failure process in the 3D rare-gas solids. From zero velocity, the crack accelerates smoothly by brittle fracture along the (110) plane until it approaches 0.36 of the Rayleigh sound speed. At this point, a dynamic instability in the brittle fracture process occurs. The brittle nature of this failure process marginally exists for the perfect (110) planar cleavage, and the deviation from planar cleavage gives rise to plasticity and a spontaneous proliferation of dislocations.

Finally, we scale the crack distance in figure 18 by the square root of enhanced strain  $\delta\epsilon$  beyond  $\delta T_s = 0$ ;  $\delta\epsilon = 1.2, 1.35, 1.6$  for  $\delta T_s = 9, 16, 27$ . In figure 19 we note that the dynamical histories approximately collapse on to a common curve. Such a scaling would be expected from continuum fracture theory.

#### 4.2. The hyperelasticity of brittle versus ductile failure [19]

In figure 20, snapshot pictures of the failure dynamics are presented for two notched surfaces, a (110)[110] notch (i.e. a notch on a (110) face growing in a [110] direction) and a (111)[110] notch. Their failures are very different. For the (110) notch, the solid fails as a brittle solid at the notch tip with planar cleavage of the bonds between the two (110) neighbouring atomic sheets defined by the initial notch, and the brittle crack continues until it passes through the entire length of the slab. There is no ‘brittle-to-ductile transition’ because the applied load does not allow the crack to reach the critical speed. For the (111) notch, the failure is immediately ductile, by plastic deformation and the emission of dislocations travelling first along an inclined (132) plane, which seems to be a secondary slip plane for FCC crystals, and then along oblique (111) slip planes. In figure 20, the dislocations are seen as slip *strings* flying from the crack tip of the (111) notch.

It is known that FCC crystals are typically ductile, irrespective of whether they are a rare-gas solid or a metal [6]. However, we find that the rare-gas solid cleaves as a brittle solid for a notch on a (110) face growing in a [110] direction. According to the existing theories of fracture [20, 21], cleavage-like brittle fracture tends to occur along crystal planes with lowest surface energy, crack orientations with highest resistance to slip and crack orientations with lowest shear stresses along available systems. Given their low slip resistance, it is surprising that an FCC solid of rare-gas atoms could brittle fracture at all. It is even more surprising, from a fundamental consideration, that the (110)[110] crack is brittle and the (111)[110] crack is ductile because the (111)[110] turns out to be the preferred orientation for brittle fracture on all accounts listed above, as shown by the following facts [19].

- (i) Classical Griffith theory predicts that the crack with the lower surface energy will be the most likely candidate for brittle fracture (the cleavage plane). The surface energies for

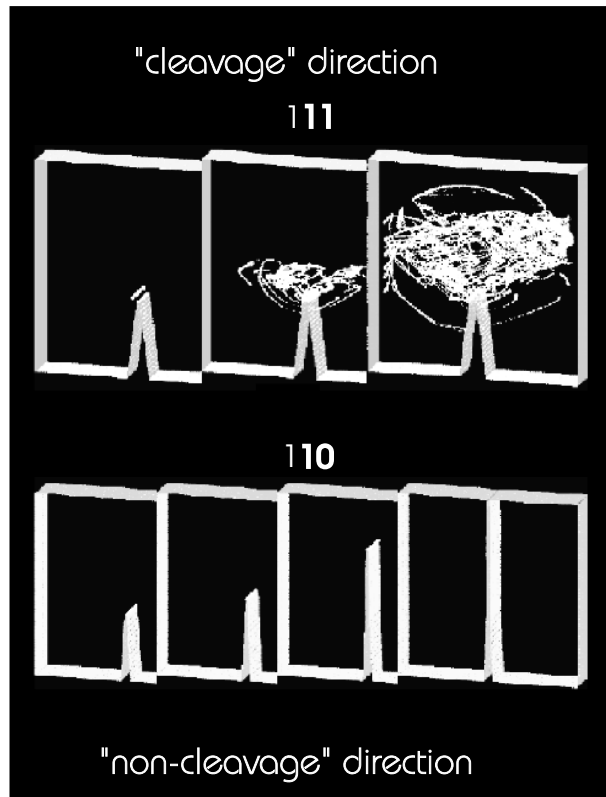


**Figure 20.** A time sequence of the propagating crack is shown as overlapping landscapes of the growing surface due to brittle fracture or ductile failure for two notch surfaces; (111) and (110). Only atoms with a cohesive energy less than 97% of the bulk value are displayed, resulting in the selected visualization of atoms neighbouring surfaces and dislocations.

the (111) and (110) faces are in the ratio 2.31:2.4. This prediction is in contradiction to the simulation result.

- (ii) Brittle fracture is likely to occur on crack orientations with highest resistance to dislocation emission since ductile versus brittle behaviours may be regarded as a competition between emission and cleavage decohesion [20, 21]. Modes of dislocation nucleation from a crack tip depends on how the slip planes cut the crack edge for a particular crack face, the primary slip system for the FCC crystal being (111)[110]; they may be inclined or oblique with respect to a chosen crack orientation. An inclined slip plane emanates from, and is coplanar with, the crack edge, and it is known that an inclined slip plane presents a much lower barrier for dislocation emission than an oblique plane (see figure 21). Using the linear elastic crack tip field as a first approximation, we can estimate the normalized resolved shear stresses, called the Schmid factors, along all the primary slip systems (figure 22). We find that the Schmid factor is larger for the (110)[110] crack. The Schmid factor calculations favour brittle cleavage on the (111)[110] orientations because the driving force for dislocation emission which is proportional to the Schmid factor is smaller for (111)[110]. This is again in contradiction with the simulation results.

In order to explain our finding, we propose that the competition between bond breaking



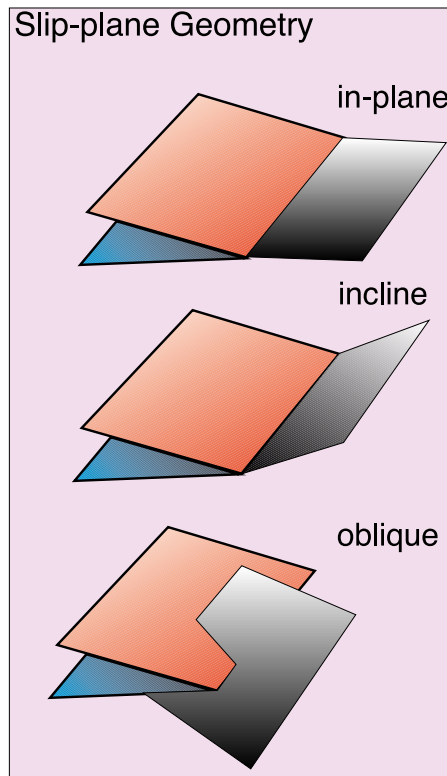


**Figure 21.** The different ways a slip plane may intersect the crack edge.

and interplanar slippage should be correlated with the behaviour of crystals near their cohesive limit (hyperelasticity). An important fact of brittle fracture is that large deformation inevitably occur in the process of bond rupture. This hyperelasticity nature of crack tip deformation must be accounted for in order to improve the continuum description of fracture. While the FCC solid is approximately isotropic in the linear elastic regime, it is highly nonlinear and anisotropic near the cohesive limit, a feature that is not generally accounted for in fracture mechanics. The hyperelasticity aspect of brittle failure can be seen from the behaviour of a bulk material subject to a uniform stretch to failure, similar to our previous calculations of two-dimensional fracture. The cohesive stress associated with stretch in a given crystal direction roughly correlates with the maximum level of stress at a crack tip perpendicular to that orientation. The smaller the cohesive stress, the more likely brittle cleavage is to occur in that orientation. In figure 23, the stress–strain curves show a pronounced elastic anisotropy at large strains for the FCC packing of simple atomic homogeneous systems (no crack). These curves are presented as Cauchy stress versus Lagrangian strain for the three-dimensional LJ lattice for uniaxial stretching in the  $[111]$  and  $[110]$  directions. The elastic properties under large deformations are highly anisotropic. The cohesive stress in the  $[111]$  direction is about 20% larger than that in the  $[110]$  direction. This difference becomes even larger if the confining stresses in the lateral directions are relaxed, as shown in figure 23. The implication of these calculations is the following: if you want to break a perfect crystal by stretching and you want to use the least effort, try the  $[110]$  direction.

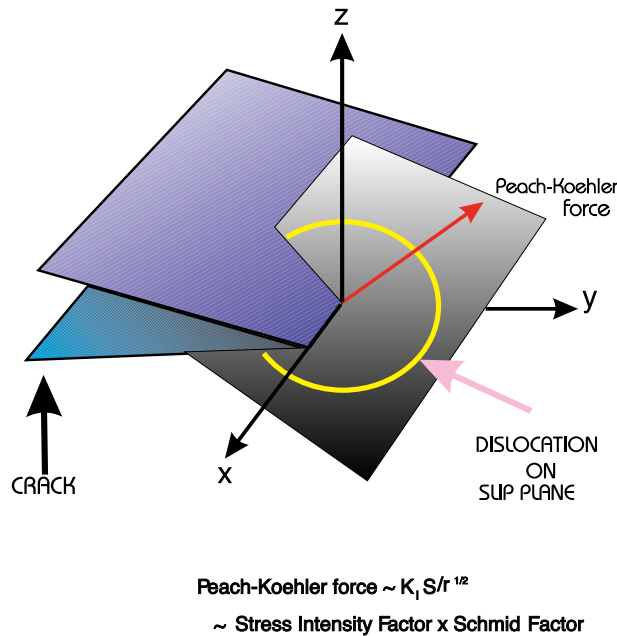


**Figure 22.** The geometry for calculating the Schmid factor.

How can we rationalize our results with the existing theories of fracture? We believe that a uniformly stretched lattice approximates the local atomic environment at the crack tip at rupture more closely than the simple energy to cut bonds bridging two neighbouring planes as in the Griffith picture. The Griffith analysis is essentially an equilibrium analysis based on a balance between the strain energy relieved at the crack tip and the surface energy created along the newly formed fracture surfaces. This balance is valid if the fracture process is quasistatic. However, during a dynamic failure process, part of the strain energy released at the crack tip region is converted into kinetic energy being transported away from the tip via stress waves and phonons. Fracture occurs as a strain localization as the cohesive stress limit is reached. Such hyperelasticity aspects of fracture are not accounted for in the existing theory of fracture. The discrepancy between theory and simulation can be explained by the hyperelasticity behaviours of solids which exhibit anisotropy in cohesive stresses in the [110] and [111] directions. A small cohesive stress means that it is more difficult to attain the critical shear stress for dislocation nucleation before the tensile stress for failure has been reached. The cohesive stress for (111) cleavage is larger than for (110) cleavage and the critical shear stress pre-empted brittle failure at the notch for this face. This delicate competition between atomic separation and atomic slippage is exhibited in our *model* material and may have profound implications for other material systems.

Hyperelasticity may be appreciated in the following simple scenario. We consider a chain of atoms being stretched toward its fracture limit. The slope of the force–displacement (or stress–strain) curve decreases continuously from its initial value corresponding to the Young’s modulus of the chain, and ultimately vanishes at the cohesive limit of the chain. Can a linear theory assuming constant elastic stiffness be used to describe the entire process of this stretching to fracture? The answer is clearly negative if our interest is to investigate the state of the chain near its failure point. Elastic softening due to hyperelastic stretching

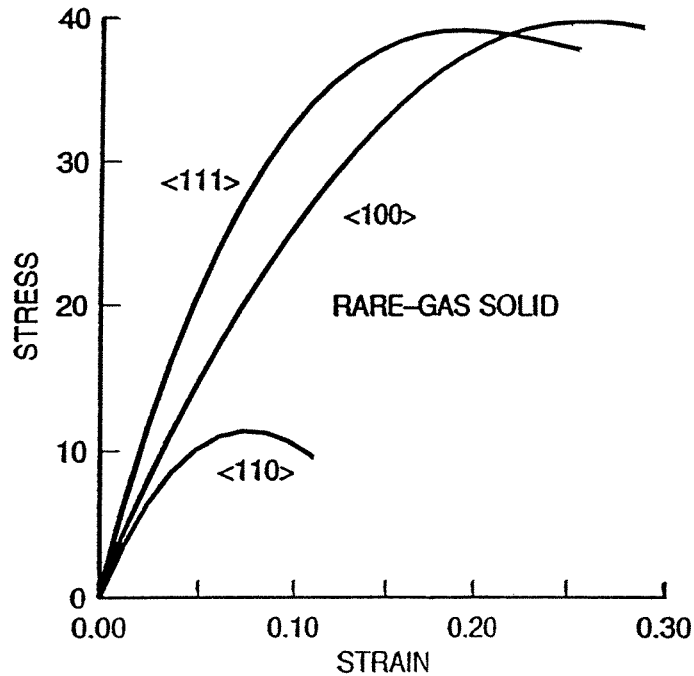


**Figure 23.** The stress–strain curves for the three-dimensional FCC rare-gas lattice for uniaxial stretching in the  $[111]$  and  $[110]$  directions. Uniaxial instability: 8% strain at 11 bars for  $\langle 110 \rangle$ ; 19% strain at 38 bars for  $\langle 111 \rangle$ ; 30% strain at 40 bars for  $\langle 100 \rangle$ .

can drastically change the way elastic waves propagate in a solid. To illustrate this point, let us consider how a long-wavelength signal propagates along a one-dimensional atomic chain stretched toward its cohesive limit. Before the chain is stretched, it behaves as an elastic bar along which a longitudinal wave signal can be transmitted with speed equal to  $\sqrt{E/\rho}$  where  $E$  denotes the Young's modulus and  $\rho$  the density of the chain. As the chain is stretched near its cohesive (fracture) limit, the tangent stiffness vanishes while a finite tension has built up with magnitude equal to the cohesive stress  $\sigma_{\max}$ . At this point, the chain behaves as an elastic string along which a transverse wave signal can be transmitted with speed equal to  $\sqrt{\sigma_{\max}/\rho}$ . Note that the cohesive-state wave speed depends on the magnitude of the stress rather than the slope of the stress–strain curve.

We have investigated the effect of hyperelasticity in the propagation of elastic waves near the cohesive limit of a two- and three-dimensional solid [22]. Elastic waves govern the speed of energy transport in a solid and it can be argued that the crack propagation velocity is limited by how fast the strain energy can be transported ahead of the crack tip to sustain the bond-breaking processes in the fracture process zone. From this point of view, the cohesive-state wave speed leads to the concept of local limiting fracture speed. For a mode I crack propagating along a straight mirror path, the stress state in front of the crack is approximately equibiaxial. We have found that the wave speed near equibiaxial cohesive stress is equal to  $\sqrt{\sigma_{\max}/\rho}$ . This behaviour resembles that of wave propagation along a one-dimensional string under tension. Taking some typical numbers for the cohesive strength and Poisson ratio as  $\sigma_{\max} = E/30$  and  $\nu = \frac{1}{4}$ , we estimate that the cohesive-state

wave speed is around 32% of the Rayleigh wave speed. This is precisely the speed at which mirror–mist crack tip instability is observed in experiments [5] and in molecular dynamic simulations discussed in this paper.

An animation of this atomistic simulation of fracture is available via the World Wide Web at the address <http://www.almaden.ibm.com/st/> and then choosing ‘visualization of fracture dynamics’.

## 5. Coupling the size scales: MAAD fracture of silicon

*What is shown:* we discuss the MAAD effort to develop techniques that bring together the continuum, atomistic and quantum descriptions in a seamless union. This is a preliminary discussion of ongoing research.

For the practical needs of the engineer trying to prevent materials failure, the simulation of ‘real’ structures on much larger space and scales must be realized. One way of achieving this, particularly the length scale issue, is by bringing together continuum, atomistic and electronic structure descriptions into a seamless union. By ‘electronic structure’ we mean the quantum description of the system of electrons and nuclei that comprise the system. The continuum description, used successfully by the applied mechanics community for decades, is proper except in the region of rapidly varying strain near the crack tip. In this region, where nonlinear microscopic dynamics plays a crucial role, an atomistic description, as modelled by classical mechanics with empirical interatomic potentials, is appropriate. Lastly, in the region where bonds are breaking, such interatomic force laws may be inadequate. In these very local regions, a quantum description of the electronic structure, which can be used to evaluate the forces on the nuclei, is required.

A project called MAAD (macro atomistic *ab initio* dynamics) has been created to accomplish a union of the ‘macro-, meso- and micro-scope’ descriptions of matter, all in a seamless way. We view this as the ‘holy grail of computational science’. The members of the MAAD Coalition are J Q Broughton at Naval Research Laboratory, E Kaxiras at Harvard University, F F Abraham at IBM Almaden Research Center and their selected colleagues. Figure 24 illustrates MAAD’s natural spatial decomposition for studying a single crack.

The first MAAD application is the rapid brittle fracture of a silicon slab flawed by a microcrack at the centre of the system which is under uniaxial tension. In the ‘far-field’ regions (macro region in figure 24) we have a continuum as implemented by the well known finite-element (FE) procedure. This macroscopic description merely needs the constitutive law for a material under study—the elastic constants suffice for our application. One processor is used per FE region. Around the crack (meso region), with large strain gradients but with no bond rupture, we use a molecular dynamic (MD) description for the atomic motion. Because MD has a large computational burden, we partition this region spatially onto several processors (just as we did for the pure MD work described in the earlier part of this paper). Lastly, in the region of bond failure, such as at the crack tip (micro region), we use a quantum mechanical description, called tight-binding (TB). Tight-binding refers to a semi-empirical electronic structure description of matter. It allows forces to be evaluated on each atom. It is the fastest numerical quantum method which contains electronic structure information; its raw input involves electrons and nuclei. But rather than evaluating costly integrals (as in much more computationally expensive *ab initio* quantum procedures), it uses predetermined matrix elements for the material under study. (The matrix elements are integrals over basis functions on different sites which describe the hopping of an electron from one atomic site to the next.) Nevertheless, the TB region is still the most

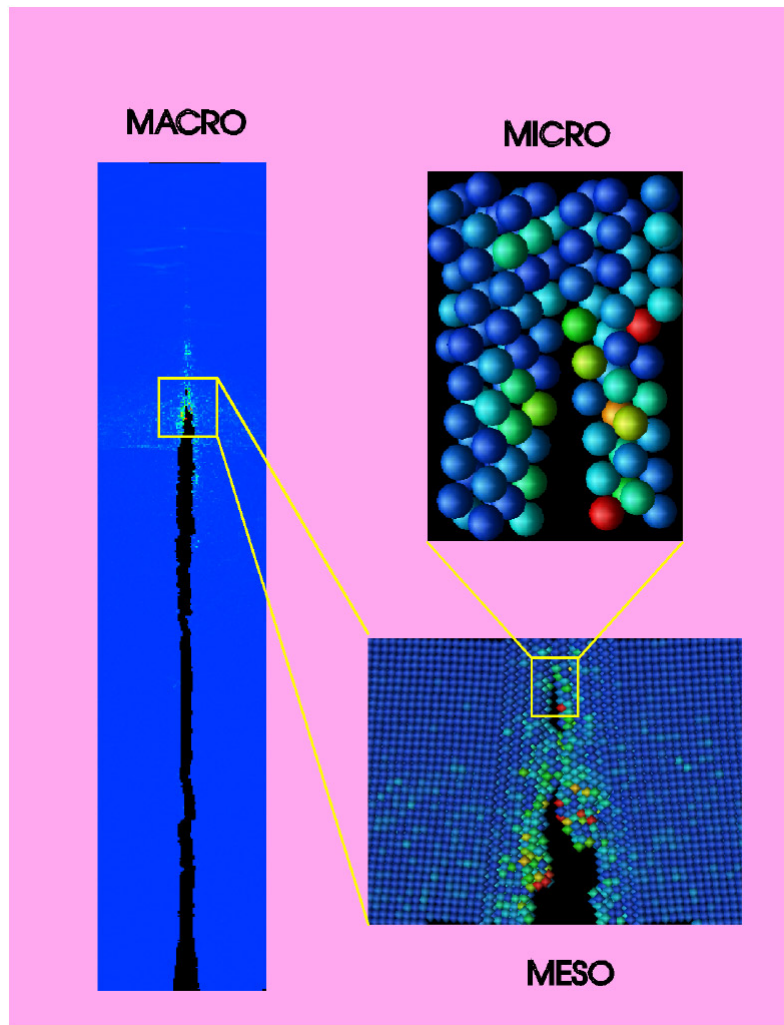


**Figure 24.** The MAAD Coalition is developing techniques that bring together the continuum, atomistic and quantum descriptions in a seamless union.

computationally complex part of the overall code and small TB regions must be used so as to ensure overall load balancing. For extended regions of bond rupture, we use overlapping TB regions.

To ensure overall consistency, we make sure that the linear elastic constants in all three regions are the same. This is the easy part. But, the two crucial, yet difficult, parts in our MAAD algorithm are clearly the handshaking between the FE and the MD and between the MD and the TB. In the FE–MD handshake region we shrink the FE mesh spacing down to atomic dimensions so that it coincides with the atomic lattice. The FE region has displacements associated with each mesh point. Since the FE region follows a Hamiltonian due to continuum elasticity theory, we can employ an update algorithm identical to that used in conventional MD so that the displacements now are dynamical variables which follow in lock-step with those of their atomic cousins in the MD region.

Since the FE mesh in the FE–MD region is of atomic dimensions, it becomes academic as to whether we think of the displacements here as atoms or ‘chunks’ of matter (‘chunks’ being a continuum concept). The FE–MD interface is always in the ‘far-field’ region where there is no diffusion. Thus atoms are unambiguously tied to lattice sites. At the beginning of the simulation, we determine which atoms are going to sit on which side of the FE–MD boundary. They remain this way for the duration of the simulation. Interactions across the FE–MD boundary are assumed to be the mean of the FE Hookian description and the MD interatomic potential description. Away from the FE–MD handshake region and moving deep into the continuum, we can make the mesh size as large as we want. Thus we can embed our atomistic simulation in as large a universe as we like. (This will solve, for example, the problem of the stress waves that emanate from a propagating crack which would reflect back from the boundaries of the MD cell in our strictly MD simulations.)

Lastly, we come to the MD–TB handshake region. Since a semiconductor system is being studied (silicon), bonding can be thought of as localized (we can treat metallic systems, but this makes the algorithm more complex). The MD–TB interface is dynamically updated at each time step. We track the path of the crack and place the centre of the TB region at the apex of the crack where most of the bond-breaking action occurs. The TB region is currently a ‘clover leaf’ of eight overlapping TB regions each of which is cylindrical. Forces on the atoms in the clover leaf are taken as the average over those predicted by the overlapping TB regions. Dangling bonds at the edge of the TB region are terminated with pseudo-hydrogens. We say ‘pseudo’ because the matrix elements which connect them to the rest of the system are carefully constructed to (i) tie off a single bond, (ii) ensure no charge transfer and (iii) place that atom at a position commensurate with the rest of the lattice. Thus at the perimeter of the MD–TB region, we have ‘hydrogens’ which sit directly on top of the atoms of the MD simulation. On one side of the TB–MD interface, we imagine that the bonds to an atom are derived from the TB Hamiltonian and on the other side the bonds are derived from the interatomic potential of the MD simulation. As before, the TB code updates atomic positions in lock-step with its FE and MD cousins. The entire MAAD algorithm is formulated in such a way that the system follows a conservative Hamiltonian.

In summary, the greatest portion of the slab is taken to be a continuum solid, and the external stresses are imposed at their extreme boundaries. In between is the MD region except where atomic bonds are stretched to failure, then the local region around the crack’s tips are described by the TB method. A simulation where the FE, MD and TB regions are working in concert is shown in figure 25. This example represents ongoing work by the MAAD Coalition to further refine the algorithms and apply them to new areas of research.

## 6. What have we learned?

We have learned there is a ‘real’ instability in rapid brittle fracture, that it is ‘dynamic’ in origin since it happens in perfect solids, that it occurs irrespective of spatial dimension and that it gives rise to a ‘dynamic brittle-to-ductile’ transition in the fragile FCC solids. We have also learned that hyperelasticity governs the dynamic failure, that it allows the FCC solid to unexpectedly fail by brittle fracture on a particular cleavage plane which violates the simple Griffith picture and in contradistinction to predictions based upon Schmid factors for slip, and that it determines whether a crack will branch and how fast it will move. Finally, we are learning how to couple the macroscopic, mesoscopic and microscopic size scales together in a seamless way.

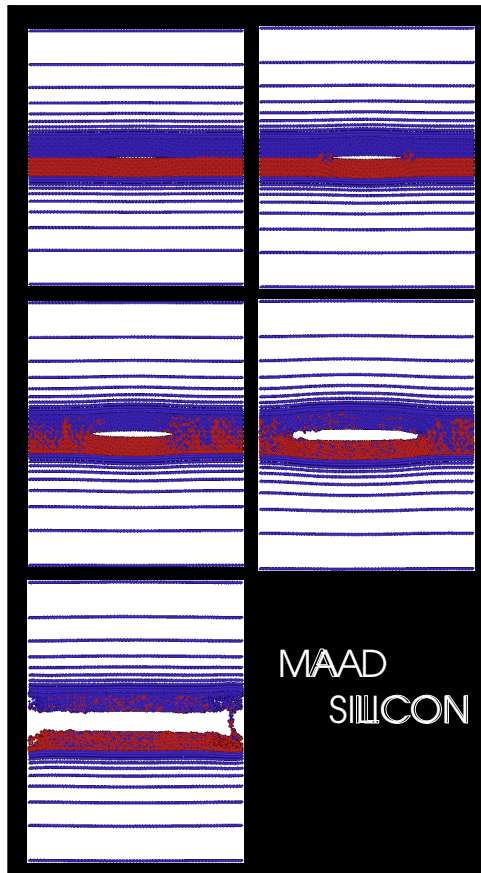


**Figure 25.** A MAAD simulation of the fracturing of a thin slab of silicon.

### Acknowledgments

Much of this research was conducted using the resources of the Cornell Theory Center, which receives major funding from the National Science Foundation and New York State.

### References

- [1] Gordon J E 1984 *The New Science of Strong Materials* (Princeton, NJ: Princeton University Press)
- [2] Herrmann H J and Roux S (eds) 1990 *Statistical Models for the Fracture of Disordered Media* (Amsterdam: North-Holland)
- [3] Freund L B 1990 *Dynamical Fracture Mechanics* (New York: Cambridge University Press)
- [4] Hoover Wm G 1991 *Computational Statistical Mechanics* (Amsterdam: Elsevier)
- Hoover Wm G, De Groot A J and Hoover C G 1992 *Comput. Phys.* **6** 155
- [5] Fineberg J, Gross S P, Marder M and Swinney H L 1991 *Phys. Rev. Lett.* **67** 457
- Fineberg J, Gross S P, Marder M and Swinney H L 1992 *Phys. Rev. B* **45** 5146
- Also see Gross S P, Fineberg J, Marder M, McCormick W D and Swinney H L 1993 *Phys. Rev. Lett.* **71** 3162
- [6] Kelly A and Macmillan N H 1986 *Strong Solids* (Oxford: Clarendon) p 10
- [7] Abraham F F, Brodbeck D, Rafey R and Rudge W E 1994 *Phys. Rev. Lett.* **73** 272
- [8] Abraham F F 1996 *Phys. Rev. Lett.* **77** 869–72

- [9] Abraham F F 1997 *Europhys. Lett.* **38** 103
- [10] Abraham F F, Schneider D, Land B, Lifka D, Skovira J, Gerner J and Rosendrantz M 1997 *J. Mech. Phys. Solids* **45** 1461
- [11] Abraham F F 1986 *Adv. Phys.* **35** 1
- [12] Bruch L W, Cole M W and Zaremba E 1997 *Physical Adsorption: Forces and Phenomena* (Oxford: Clarendon)
- [13] Auerbach D J, Paul W, Rudge W E and Abraham F F 1987 *J. Phys. Chem.* **91** 4881
- [14] Allen M P and Tildesley D J 1987 *Computer Simulation of Liquids* (Oxford: Clarendon)
- [15] Rapaport D C 1996 *The Art of Molecular Dynamics Simulation* (Cambridge: Cambridge University Press)
- [16] Plimpton S 1995 *J. Comput. Phys.* **117** 1
- [17] Abraham F F, Brodbeck D, Rudge W E and Xu X-P 1997 *J. Mech. Phys. Solids* **45** 1595
- [18] Lawn B, Hockey B and Wiederhorn S 1980 *J. Mater. Sci.* **15** 1207 figure 15(a)
- [19] Abraham F F and Gao H 1998 *Phil. Mag.* accepted
- [20] Kelly A, Tyson W and Cottrell A H 1967 *Phil. Mag.* **15** 567
- [21] Rice J R and Thomson R M 1974 *Phil. Mag.* **29** 73
- [22] Gao H 1996 *J. Mech. Phys. Solids* **44** 1453